

Article

Effects of Streamwise Sinusoidal Flow on the Aerodynamic Characteristics of a Box Girder

Haohong Li ¹, Liangliang Zhang ^{1,2,*}, Bo Wu ^{3,*} and Zhao Xiao ¹

¹ School of Civil Engineering, Chongqing University, Chongqing 400044, China; 20161602052t@cqu.edu.cn (H.L.); 20191613022t@cqu.edu.cn (Z.X.)

² Office of Scientific Research, Chongqing Metropolitan College of Science and Technology, Chongqing 402167, China

³ School of Civil Engineering, State Key Laboratory of Mountain Bridge and Tunnel Engineering, Chongqing Jiaotong University, Chongqing 400074, China

* Correspondence: 30282@cqu.edu.cn (L.Z.); bo.wu@cqjtu.edu.cn (B.W.)

Abstract: This study systematically investigated the aerodynamic characteristics of a closed box girder in sinusoidal oscillating flow fields based on experimental and numerical approaches. The numerical method was validated through comparison with experimental results. The effects of the oscillating frequencies ($KC = 0.25\sim 12$) and amplitudes ($U_m = 0.5\sim 2.0$ m/s) on the pressure distributions, total forces, and wake characteristics were investigated. The results show that the mean pressure coefficients and time-averaged streamline distributions are insensitive to the oscillating frequency and amplitude. However, the characteristics of the sinusoidal oscillating inflow significantly influence the fluctuating aerodynamic forces and the fluctuating drag forces increase linearly with the oscillating frequency. In particular, for the wake flow, the larger oscillating frequency and amplitude of the inflow led to more obvious wake vortex shedding.

Keywords: wind tunnel test; aerodynamic characteristic; closed box girder; CFD; sinusoidal flows



Citation: Li, H.; Zhang, L.; Wu, B.; Xiao, Z. Effects of Streamwise Sinusoidal Flow on the Aerodynamic Characteristics of a Box Girder. *Appl. Sci.* **2022**, *12*, 5341. <https://doi.org/10.3390/app12115341>

Academic Editor: Artur Tyliczszak

Received: 8 April 2022

Accepted: 21 May 2022

Published: 25 May 2022

Publisher's Note: MDPI stays neutral with regard to jurisdictional claims in published maps and institutional affiliations.



Copyright: © 2022 by the authors. Licensee MDPI, Basel, Switzerland. This article is an open access article distributed under the terms and conditions of the Creative Commons Attribution (CC BY) license (<https://creativecommons.org/licenses/by/4.0/>).

1. Introduction

With improvements in the level of economic development and traffic volume, the span of bridges has gradually increased [1,2]. However, large-span bridges have a lower stiffness and greater susceptibility to wind-induced vibration, which make these bridges more sensitive to wind [3]. Closed box girders are widely used in large-span bridges due to their superior aerodynamic features [4].

The research on aerodynamic characteristics of bluff bodies in sinusoidal oscillating flows covers a wide range of fields, such as wind engineering, bridge engineering, and marine engineering [5,6]. The velocity time history of a sinusoidal oscillating flow varies with a sinusoidal function and can be divided into zero-mean sinusoidal oscillating flow and non-zero-mean (unidirectional) sinusoidal oscillating flow according to the mean velocity of the flow motion [7]. In contrast to uniform flow, zero-mean sinusoidal oscillating flow has unsteady characteristics due to the acceleration and deceleration process of the flow. Compared with zero-mean sinusoidal oscillating flow, unidirectional sinusoidal oscillating flow does not exhibit reciprocating motion, and its unsteady characteristics are not as large as those of zero-mean sinusoidal oscillating flow.

In the 20th century, researchers began to study the zero-mean sinusoidal oscillating flow around a circular cylinder. In 1950, Morison et al. [8] proposed the Morison equation for calculating the drag of a cylinder by studying the flow around a cylinder under small-amplitude wave motion. Keulegan and Carpenter [9] studied the coefficients in the Morison equation and the characteristic parameter KC , which characterizes the amplitude of the oscillating flow, leading to more widespread use of the Morison equation in engineering. Williamson [10] and Obasaju et al. [11] experimentally studied the flow around a cylinder in

a sinusoidal oscillating flow. The results showed that the flow can be divided into different patterns in different KC number ranges. When $KC \ll 1$, the flow is in a two-dimensional, attached, and symmetrical state; when this critical KC number is exceeded, the flow is no longer symmetrical, and as the KC number continues to increase, various different vortex shedding patterns emerge, each corresponding to a different number of vortex sheddings in an incoming oscillation cycle.

For non-zero-mean sinusoidal oscillatory flow, researchers have conducted relevant studies using experimental and numerical methods. In 2003, Nomura et al. [12] used an active-control wind tunnel to study the forces of a square column in a non-zero-mean sinusoidal oscillatory flow with large angles of attack. The test results showed that the Morison equation can be used to investigate the drag time history of the cylinder. Chen et al. [13] simulated the forces of a square column in a non-zero-mean sinusoidal oscillatory flow using the three-dimensional LES method. Zhao et al. [14] used the DNS method to numerically simulate the flow around a cylinder in a non-zero-mean sinusoidal oscillatory flow. The results showed that the drag force of the cylinder increases with frequency in a non-zero-mean oscillating flow.

Turbulence flow can be considered as the superposition of multiple sinusoidal flow components with different amplitudes and periods [15]. Thus, investigating the single-frequency sinusoidal oscillating flow and extending it to the superposition of multiple-frequency sinusoidal flows can overcome the deficiencies in the passive turbulence simulations in previous studies, allowing for parameterized research on turbulence intensity and integral scale. So far, as shown in Table 1, studies on sinusoidal oscillating flow have focused mainly on the flow around a cylinder.

Table 1. Review of the literature on unsteady sinusoidal flow.

Reference	Geometry	Sinusoidal flow	Method	Conclusion
Morison (1950) [8]	cylinder	low frequency	wind tunnel	Morison equation
Obasaju et al. (1988) [11]	cylinder	low frequency	wind tunnel	flow patterns
Nomura et al. (2003) [12]	cylinder	low frequency	wind tunnel	aerodynamic force
Chen et al. (2010) [13]	cylinder	low frequency	CFD	aerodynamic force
Zhao et al. (2010) [14]	cylinder	low frequency	CFD	flow patterns
Ma et al. (2013) [16]	box girder	low frequency	wind tunnel	aerodynamic admittance functions
Wang et al. (2021) [17]	box girder	low frequency	wind tunnel	aerodynamic admittance functions

For large-span bridges, due to the limitations to wind tunnel setups, some studies identified the aerodynamic admittance in low-frequency sinusoidal flows [16,17]. Moreover, the mechanism of the influence of the sinusoidal flow on the aerodynamic characteristics of a bridge section has been relatively less studied. Therefore, it is necessary to conduct an in-depth study and analysis of the mechanism of the influence of sinusoidal flow on the aerodynamic characteristics of a bridge section.

This study systematically describes the effects of sinusoidal oscillating flow on the aerodynamic characteristics of a closed box girder. The numerical results were validated through wind tunnel tests. The remainder of this paper is organized as follows. Section 1 describes the experimental and numerical methods. The effects of oscillating sinusoidal flows on the pressure characteristics and total forces are studied in Sections 2 and 3, respectively. In Section 4, the flow separation and reattachment around the box girder, as well as wake patterns in different sinusoidal flow fields, are investigated using the numerical method. Our conclusions are briefly summarized in Section 5.

2. Experimental and Numerical Setups

2.1. Experimental Tests

Wind tunnel tests were conducted in the active-control wind tunnel at Tongji University, as shown in Figure 1a. The model was installed on a bracket system in the wind

tunnel. This study mainly discusses the influence of the streamwise sinusoidal flows on the aerodynamic characteristics of a closed box girder.

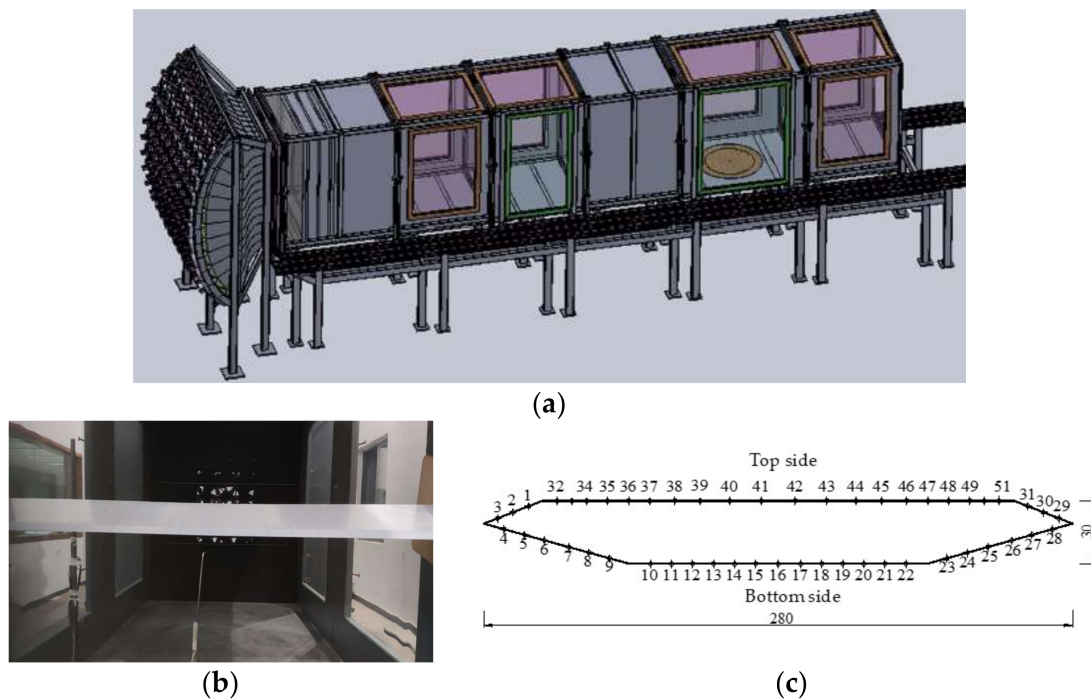


Figure 1. Wind tunnel setups. (a) active-control wind tunnel; (b) tested cross-section; (c) schematic diagram of the pressure taps (unit: mm).

The dimensions of the section model are $B = 0.28$ m (width), $D = 0.03$ m (height), and $L = 1.8$ m (length). To measure the fluctuating surface pressure, measuring taps were positioned in the center portion of the model.

Based on a multi-fan system, various harmonic flow fields with a periodic velocity oscillation in the streamwise direction were generated. The harmonic periodic velocity is defined as

$$u(t) = U + U_m \cdot \sin(2\pi \cdot f_u \cdot t) \tag{1}$$

where the mean velocity is $U = 8$ m/s for all cases in this study; U_m is the oscillation amplitude, which was set in the range of $0 \leq U_m/U \leq 0.25$; and f_u is the oscillation frequency, which was set in the range of 0.2~1.2 Hz.

2.2. Numerical Methods

2.2.1. Computational Details

The computational domain of the simulations reproduces the geometry of the box girder model at a 1:1 scale ratio, as shown in Figure 2. In order to ensure the independence of the computational domain, the distance from the top and bottom boundaries to the section center was set to $10 B$, the inlet was set to $10 B$ in front of the section center, and the outlet was set to $20 B$ behind the section center.

To numerically generate the sinusoidal oscillating flow field, boundary conditions were set to reproduce the wind tunnel test setups, as shown in Figure 2. The $k-\omega$ SST turbulence model was selected for the control equations, the deck surface was specified to have no-slip wall conditions for velocity and the Neumann condition for pseudo-pressure, the inlet was specified to have velocity-inlet conditions, and each of the generated flows in the simulations had a periodic velocity oscillation in the streamwise direction, achieved through a user-defined function (UDF) defined by $u(t) = U + U_m \cdot \sin(2\pi \cdot f_u \cdot t)$. The outlet

was specified to have outflow conditions, and the top and bottom sides were specified to have symmetry conditions.

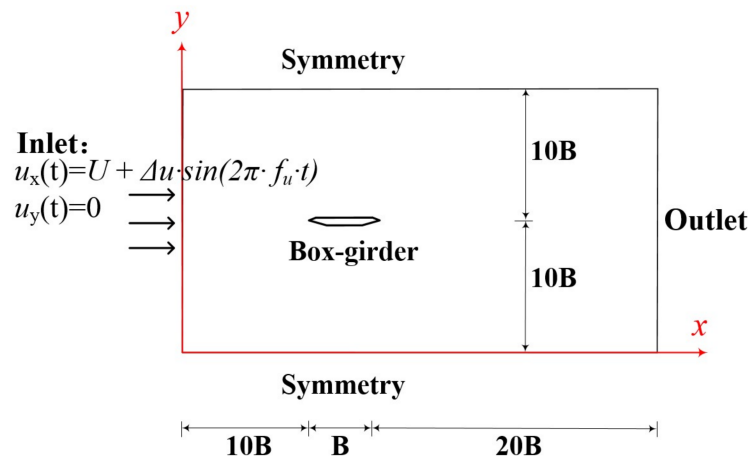


Figure 2. Computational domain and boundary conditions of the sinusoidal flow field.

In this study, the computational cases were set based on Equation (1) and the *KC* number of the numerically generated sinusoidal oscillating flows was set in the range of 0.25~12.0 [7], corresponding to a frequency range of 1.39~66.67 Hz, as shown in Table 2.

$$f_u = \frac{U_m}{KC \cdot D} \tag{2}$$

Table 2. Details of the numerical cases in the sinusoidal oscillating flow.

U_m (m/s)	0.5; 1.0; 2.0											
<i>KC</i>	0.25	0.5	1.0	2.0	3.0	4.0	5.0	6.0	8.0	10.0	12.0	
f_u (Hz)	66.67	33.33	16.67	8.33	5.56	4.17	3.33	2.78	2.08	1.67	1.39	

2.2.2. Spatial and Temporal Discretization

Structured grids were used to discretize the spatial computational domain. To ensure the quality of the grid in the boundary layer of the model, the O-Block grid was used near the deck surface with a height of 0.1 mm for the first layer. To improve the calculation efficiency, a sparse grid was used in the other areas of the grid. The maximum grid size was 0.04 m. The total number of grids was 103,099, and the mesh distributions were defined through refining tests to ensure mesh-independent solutions. The two-dimensional mesh distribution is shown in Figure 3.

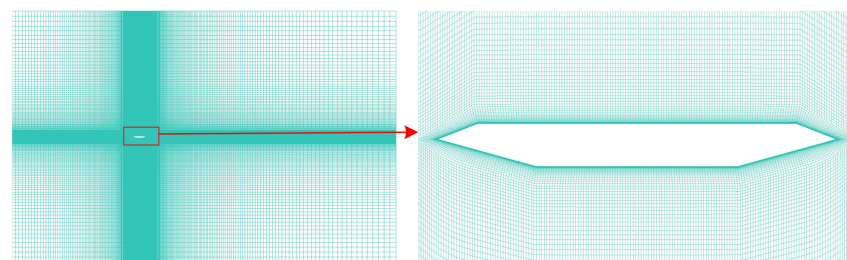


Figure 3. Meshing distributions.

Several tentative calculations were adopted to ensure the time-independence of the computational domain, and the time step was set as $\Delta t = 0.0005$ s, which provides an accurate advancement in time. For each numerical case, the simulation was fully calculated

first under uniform flow conditions and then using the UDF program to load the sinusoidal oscillatory flow boundary conditions. The data were collected after the calculation had stabilized. All the simulations were extended over $T = 20$ s to ensure convergence of the flow statistics.

2.3. Validations

The pressure coefficients are expressed as

$$C_{Pi}(t) = \frac{P_i(t) - P_\infty}{0.5\rho U^2} \quad (3)$$

where $P_i(t)$ is the time history of the fluctuating pressure at point i , P_∞ is the pressure of the reference point, and ρ is the air density. The mean and root mean square (RMS) pressure distributions of typical cases are shown in Figure 4. The numerical results are in good agreement with the experimental results; the differences between the two methods may be due to the different boundary conditions.

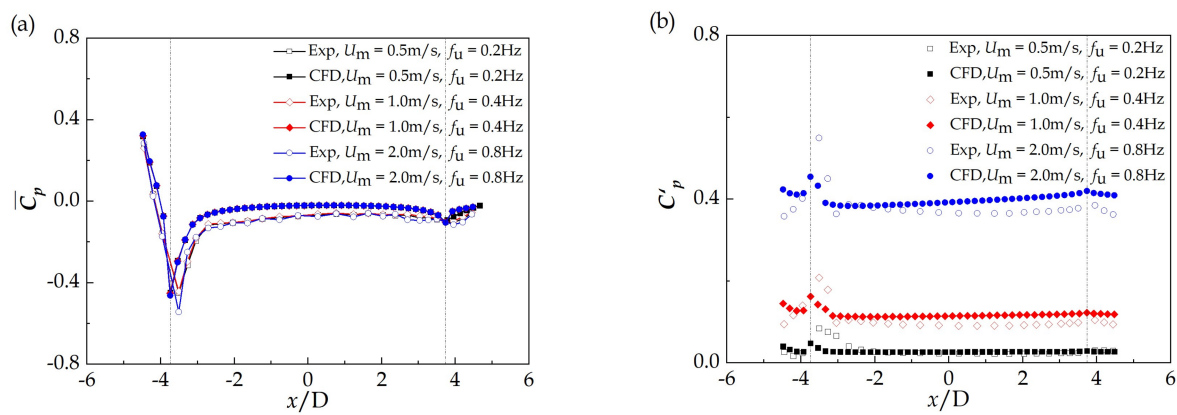


Figure 4. Comparison of numerical and experimental results in sinusoidal flow: (a) mean pressure coefficients (top side); (b) fluctuating pressure coefficients (top side).

3. Effects of Streamwise Sinusoidal Flow on Pressure Characteristics

3.1. The Pressure Characteristics

The pressure characteristics are of paramount importance and carry information about the aerodynamic loads and the aerodynamic fluctuations. Figure 5 shows the time-averaged pressure coefficients (\bar{C}_p) of the closed box girder at a null angle of attack in different streamwise sinusoidal flows. Cases with different frequencies (f_u) and the same amplitude (U_m) are compared in the same figure.

It is obvious that f_u has no significant effect on \bar{C}_p on either side of the model at low oscillating amplitudes ($U_m = 0.5\text{--}1.0$ m/s). At a larger oscillating amplitude ($U_m = 2.0$ m/s), slight changes were observed in \bar{C}_p at large oscillating frequencies ($f_u = 33.33\text{--}66.67$ Hz). Thus, it can be concluded that the time-averaged pressure distributions of the box girder are insensitive to the oscillating frequency and amplitude of the streamwise sinusoidal flows.

A comparison of the RMS pressure forces (C'_p) on the top and bottom surfaces of the girder in different sinusoidal inflows is shown in Figure 6. Cases with different frequencies and the same amplitude are compared in the same figure. For the same amplitude, the C'_p increases significantly with the increasing oscillating frequency, and the higher the amplitude, the more obvious the change in the RMS pressure force. A similar result is obtained by comparing cases with different U_m values at the same f_u , indicating that the C'_p increases with increasing f_u and U_m in streamwise sinusoidal flows.

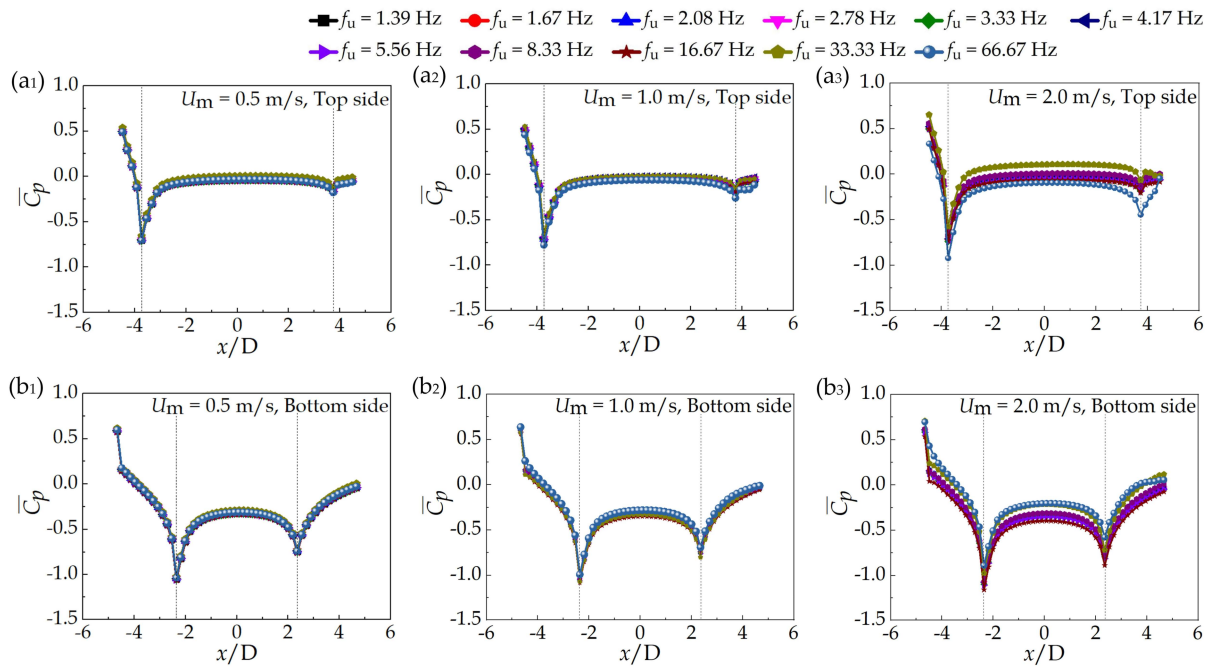


Figure 5. Mean pressure coefficients in streamwise sinusoidal oscillating flows: (a₁) $U_m = 0.5$ m/s, top side; (a₂) $U_m = 1.0$ m/s, top side; (a₃) $U_m = 2.0$ m/s, top side; (b₁) $U_m = 0.5$ m/s, bottom side; (b₂) $U_m = 1.0$ m/s, bottom side; (b₃) $U_m = 2.0$ m/s, bottom side.

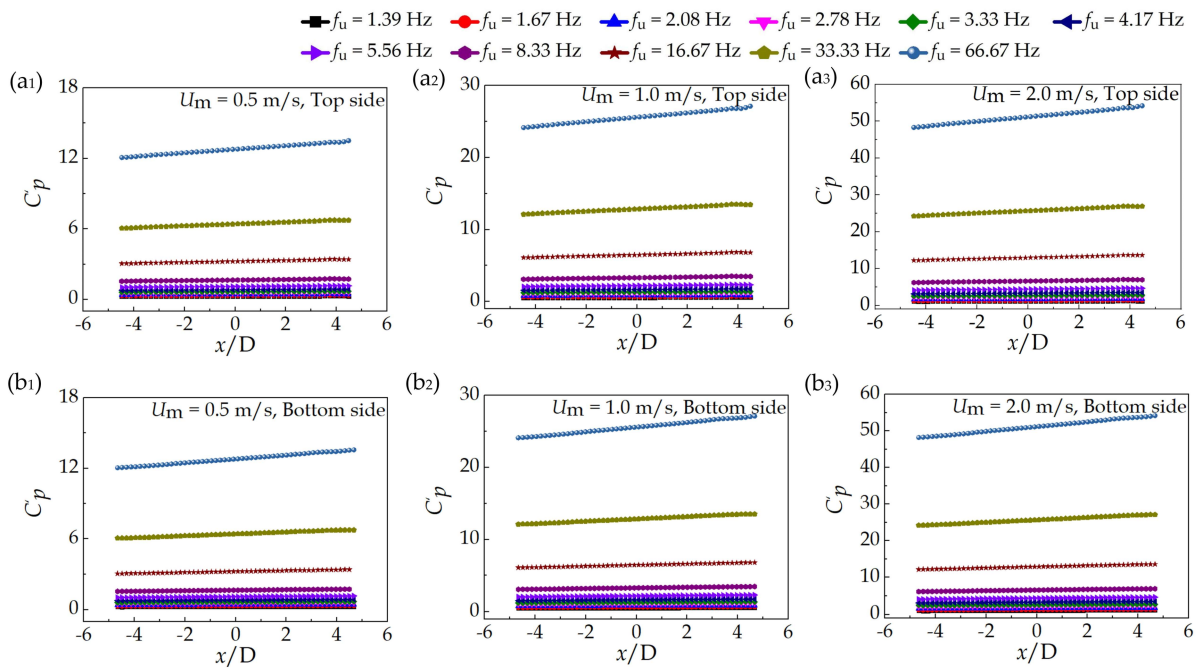


Figure 6. RMS pressure coefficients with different f_u and U_m values in streamwise sinusoidal oscillating flows: (a₁) $U_m = 0.5$ m/s, top side; (a₂) $U_m = 1.0$ m/s, top side; (a₃) $U_m = 2.0$ m/s, top side; (b₁) $U_m = 0.5$ m/s, bottom side; (b₂) $U_m = 1.0$ m/s, bottom side; (b₃) $U_m = 2.0$ m/s, bottom side.

Figure 7 presents the variation trend of the RMS pressure coefficient (C'_{P0}) at the stationary point ($x = -0.14, y = 0$) of the closed box girder in different sinusoidal flow fields. It is shown that a larger U_m produces a larger C'_{P0} . In addition, C'_{P0} is proportional to the frequency at the same amplitude. It can be concluded that the RMS pressure coefficient at

the stationary point of the closed box girder is related to the amplitude and frequency of the streamwise sinusoidal oscillating flows.

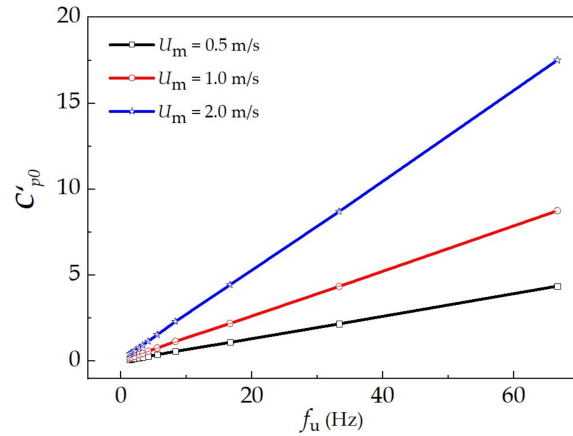


Figure 7. RMS pressure coefficients at the stationary point ($x = -0.14, y = 0$) in the streamwise sinusoidal oscillating flows.

For the same U_m and f_u , the values of C'_p increase linearly along the box girder surfaces in oscillating flows, as shown in Figure 6. To observe this trend directly, Figure 8 presents the distribution of the normalized RMS pressure coefficient (C'_p/C'_{p0}). The results show that there is a mutation of C'_p/C'_{p0} at the corners of the box girder, and the values of C'_p/C'_{p0} change linearly along the bridge section when $f_u \leq 4.17$ Hz. For a higher f_u , the curve shows a linear trend along the entire bridge section; the corners of the box girder have a slight impact on the normalized RMS pressure coefficient.

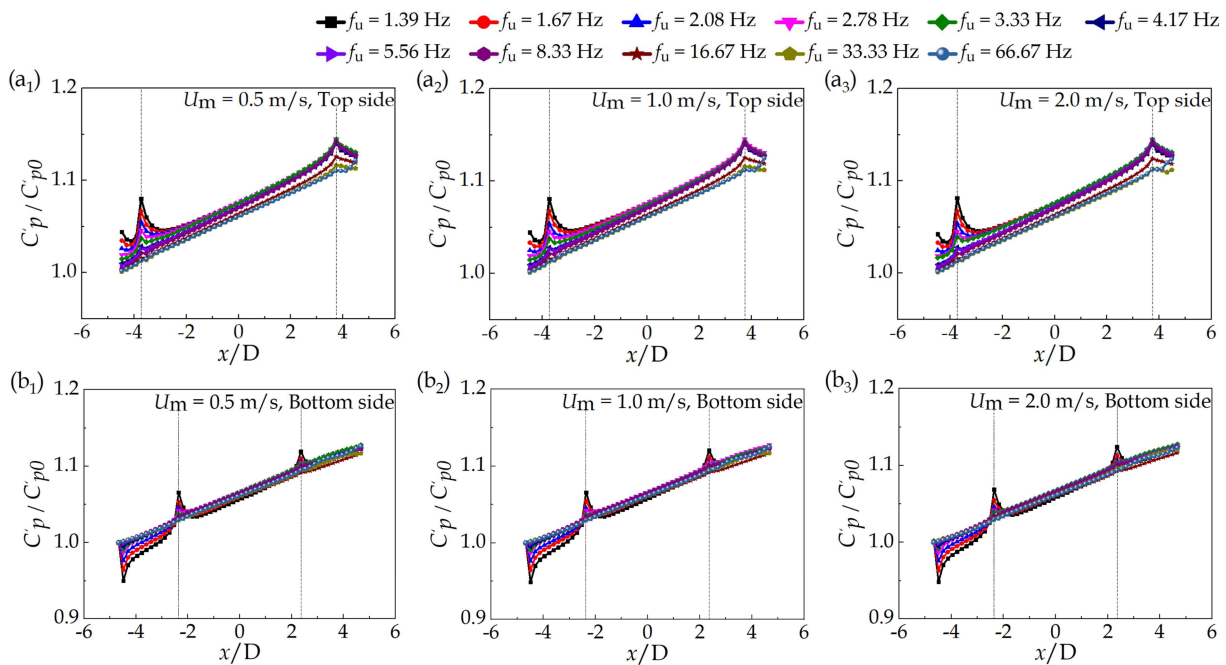


Figure 8. Normalized RMS pressure coefficients in the streamwise sinusoidal oscillating flows: (a₁) $U_m = 0.5$ m/s, top side; (a₂) $U_m = 1.0$ m/s, top side; (a₃) $U_m = 2.0$ m/s, top side; (b₁) $U_m = 0.5$ m/s, bottom side; (b₂) $U_m = 1.0$ m/s, bottom side; (b₃) $U_m = 2.0$ m/s, bottom side.

It can be concluded that the normalized RMS pressure coefficients on both sides of the girder in sinusoidal oscillating flows are related only to the oscillating frequency.

3.2. Streamwise Correlations

The streamwise correlation of the pressure coefficient is defined as

$$R_{pp}(x, x_0) = \frac{\overline{P_x P_0}}{P'_x P'_0} \tag{4}$$

where P_x is the pressure of tap x , P_0 is the pressure at $x/B = -0.5$, the overbar indicates a time-averaged quantity, and P'_x and P'_0 are the standard deviations of P_x and P_0 , respectively.

To investigate the frequency and phase characteristics of all measurement points of the box girder surface, the streamwise correlation (R_{pp}) on the box girder surface in different streamwise sinusoidal flows is shown in Figure 9. The reference point is set at the stationary point ($x = -0.14, y = 0$). For a low frequency, the streamwise sinusoidal flow is attached to the wind nose and inclined web when it passes through the stationary point; there is a deviation between the flows and the dominant wind direction. Accordingly, the values of R_{pp} tend to decrease along the wind nose and inclined web on the windward side. After the flow passes the corners of the bridge surface, the R_{pp} is recovered because the flow adheres to the top and bottom surfaces in the same direction. R_{pp} begins to decline again as the flow reattaches to the wind nose and inclined web of the leeward side. The flow separates from the box girder surfaces, returns to the dominant wind direction, and the value of R_{pp} gradually recovers in the wake region.

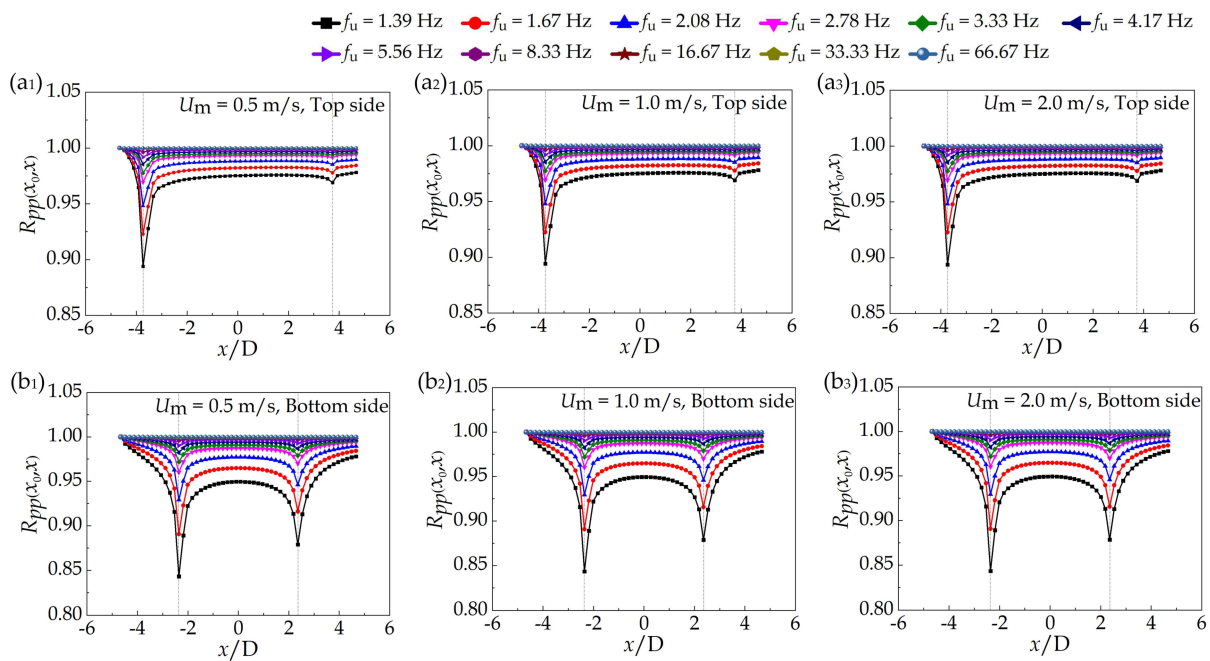


Figure 9. Streamwise correlation of pressure coefficients in streamwise sinusoidal flows: (a₁) $U_m = 0.5$ m/s, top side; (a₂) $U_m = 1.0$ m/s, top side; (a₃) $U_m = 2.0$ m/s, top side; (b₁) $U_m = 0.5$ m/s, bottom side; (b₂) $U_m = 1.0$ m/s, bottom side; (b₃) $U_m = 2.0$ m/s, bottom side.

Comparing the effects of different oscillating flows, it is observed that the streamwise correlation of both sides increases with increasing frequency. When the f_u increases to 8.33 Hz, the distribution of R_{pp} along the box girder is approximately a straight line, which can be considered as unity.

Three typical frequencies were selected to quantify the R_{pp} of the box girder, and the comparison results are shown in Figure 10. It can be observed that the oscillating amplitude has no significant impact on the R_{pp} . However, the R_{pp} is sensitive to the oscillating frequency.

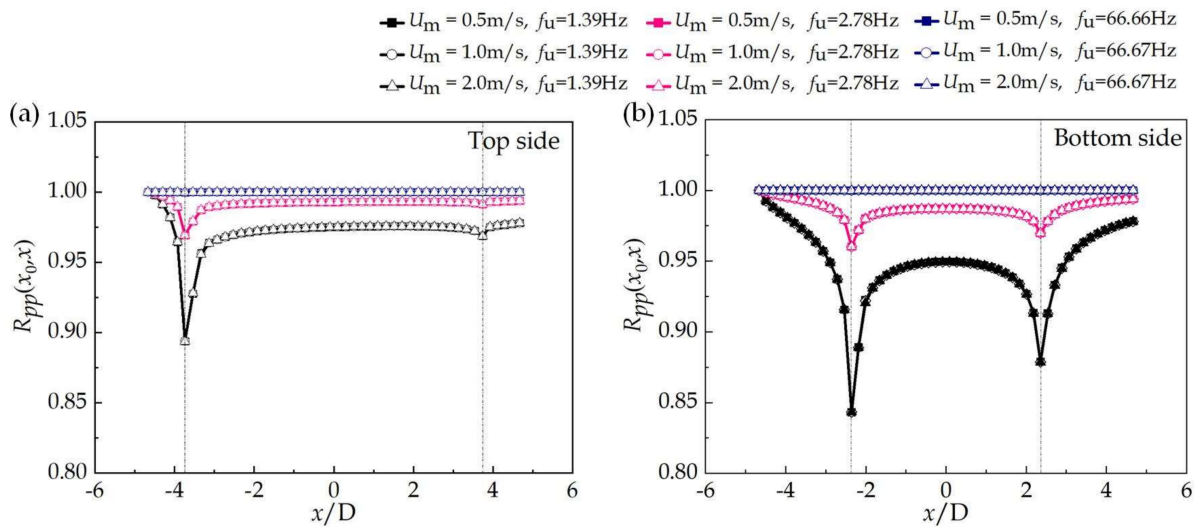


Figure 10. Streamwise correlations of pressure coefficients with different U_m values in streamwise sinusoidal flows: (a) top side; (b) bottom side.

3.3. Non-Gaussian Features

The skewness (sk) of the pressure coefficient reflects the probability density distribution of the wind pressure coefficient. To investigate the time-domain features of the surface pressure in sinusoidal oscillating flows, Figure 11 shows the distribution of the third-order statistical central moments of pressure in the form of skewness, which is defined as

$$sk = \frac{1}{n-1} \sum_{i=1}^n (C_{pi} - \bar{C}_p)^3 / (C'_p)^3 \quad (5)$$

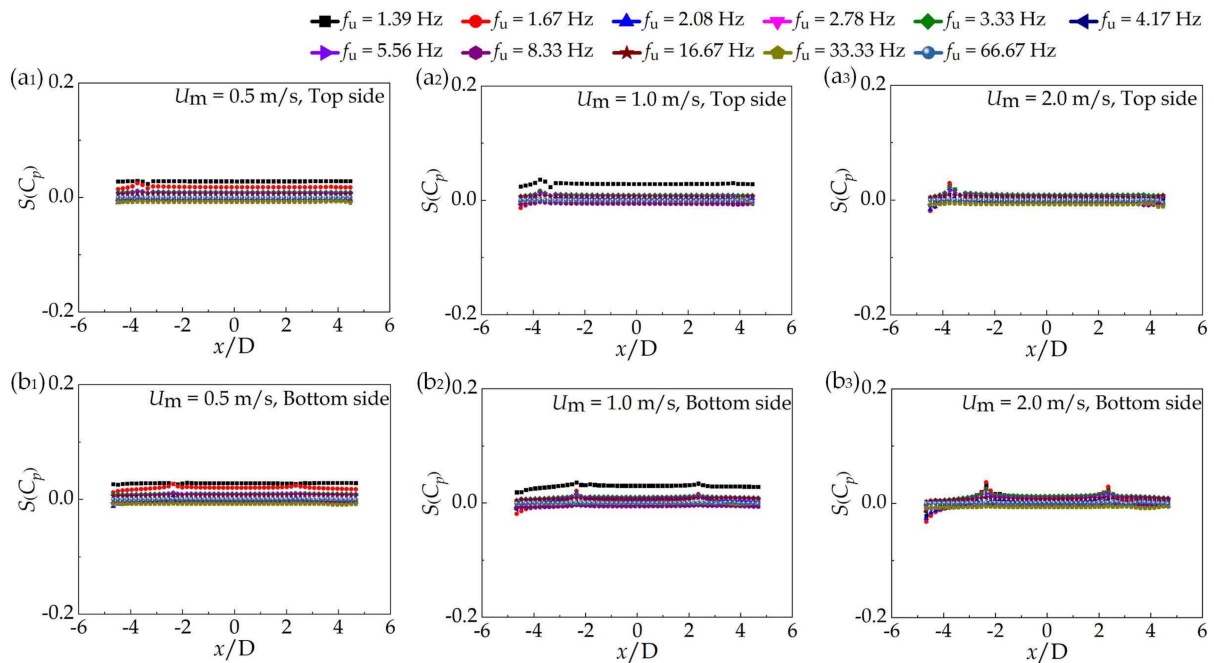


Figure 11. Skewness of pressure coefficients in the streamwise oscillating flows: (a₁) $U_m = 0.5$ m/s, top side; (a₂) $U_m = 1.0$ m/s, top side; (a₃) $U_m = 2.0$ m/s, top side; (b₁) $U_m = 0.5$ m/s, bottom side; (b₂) $U_m = 1.0$ m/s, bottom side; (b₃) $U_m = 2.0$ m/s, bottom side.

As shown in Figure 11, the inflow frequency has little effect on the peak value of sk . Thus, the surface pressure in the time domain can still be considered as a Gaussian distribution. This phenomenon is related to the flow separation characteristics in that there is no noticeable flow separation around the closed box girder in all sinusoidal flow fields with different frequencies and amplitudes.

4. Effect of Streamwise Sinusoidal Flow on Total Forces

4.1. Mean and RMS Forces

The mean and RMS aerodynamic forces of the box girder in various sinusoidal oscillating flow fields with different oscillating amplitudes and oscillating frequencies are shown in Figure 12. It can be observed that for the sinusoidal flow field with a small oscillating amplitude ($U_m = 0.5$ m/s), the aerodynamic forces vary relatively little with respect to the oscillating frequencies. However, for the sinusoidal flow fields with larger oscillating amplitudes ($U_m = 1.0$ m/s and $U_m = 2.0$ m/s), the aerodynamic forces vary dramatically with respect to increasing f_u values.

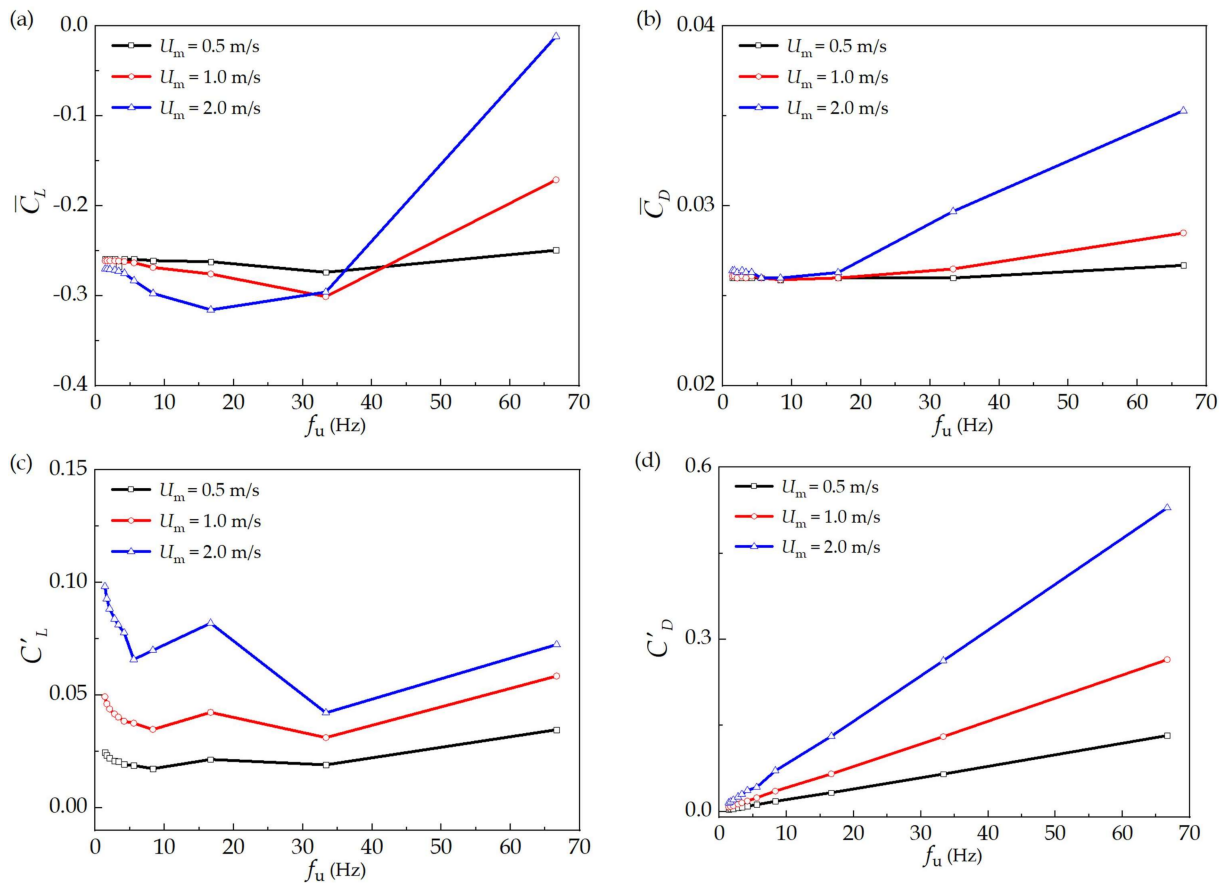


Figure 12. Mean and RMS aerodynamic force of the girder in streamwise oscillating flows: (a) mean lift force; (b) mean drag force; (c) RMS lift force; (d) RMS drag force.

For the mean lift coefficient (C_L) of the box girder, it remains essentially constant in the flow field with $U_m = 0.5$ m/s. However, C_L decreases with the oscillating frequencies and then increases at high frequencies in the flow fields with $U_m = 1.0$ m/s and $U_m = 2.0$ m/s. Moreover, for the RMS lift coefficient (C'_L) of the box girder, it varies significantly with respect to increasing oscillating frequencies, indicating that the oscillating frequency has notable effects on the aerodynamic lift force, and that it is the larger oscillating amplitude of the sinusoidal flow fields that has the more apparent effects.

For the mean drag coefficient (C_D) of the box girder, it shows no apparent variation in the low-frequency sinusoidal flows ($f_u \leq 8.33$ Hz). It is not until the oscillating frequency

increases to 16.67 Hz that the mean drag force increases obviously, and the higher the oscillating amplitude the more pronounced the change in the mean drag force. Furthermore, for the RMS drag coefficient (C'_D) of the box girder, it is linearly related to the oscillating frequencies. The linear relationship between C'_D and U_m can also be observed by comparing the curves at the same f_u .

4.2. Frequency Domain Features

The spectrum of the lift force (a_1 – c_1) and drag force (a_2 – c_2) in typical cases is shown in Figure 13 to analyze the influence of sinusoidal oscillating flows on the bridge frequency domain features. Comparing the values of the reduced frequency (f/f_u), it is found that the spectrum of C_D has only one peak value corresponding to a certain f_u . The predominant frequency of the spectrum of C_L corresponds to the inflow frequency f_u . Moreover, in the sinusoidal flows with larger oscillating amplitudes and frequencies, multiple predominant frequencies can be found in the lift spectrum, which may be due to the secondary effect of the wake flow.

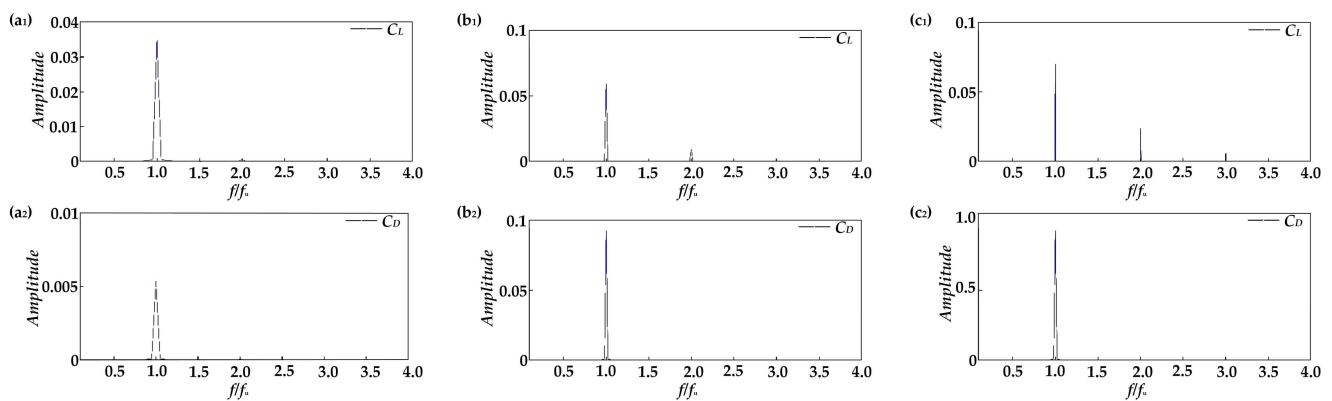


Figure 13. Spectrum of C_L and C_D in different sinusoidal oscillating flows: (a₁,a₂) $U_m = 0.5$ m/s, $f_u = 1.39$ Hz; (b₁,b₂) $U_m = 1.0$ m/s, $f_u = 16.67$ Hz; (c₁,c₂) $U_m = 2.0$ m/s, $f_u = 66.67$ Hz.

5. Effects of Streamwise Sinusoidal Flow on Separated Flow

5.1. Flow Separation and Reattachment

The formation of aerodynamic force is greatly affected by flow separation and reattachment [3]. To study the characteristics of the flow separation of the box girder in sinusoidal oscillating flows, Figure 14 presents the time-averaged stream line distributions in different streamwise sinusoidal flows. It can be observed that the flow around the box girder is tightly attached to the box section in all uniform flows and sinusoidal flows, benefitting from the large aspect ratio ($B/D = 9.3$) of the box girder. It should be noted that the stream line distributions in the sinusoidal flows are nearly the same as those in the uniform flow [3]. In other words, the oscillating amplitudes and frequencies of the streamwise sinusoidal flow have no obvious impact on the time-averaged stream line distributions around the box girder.

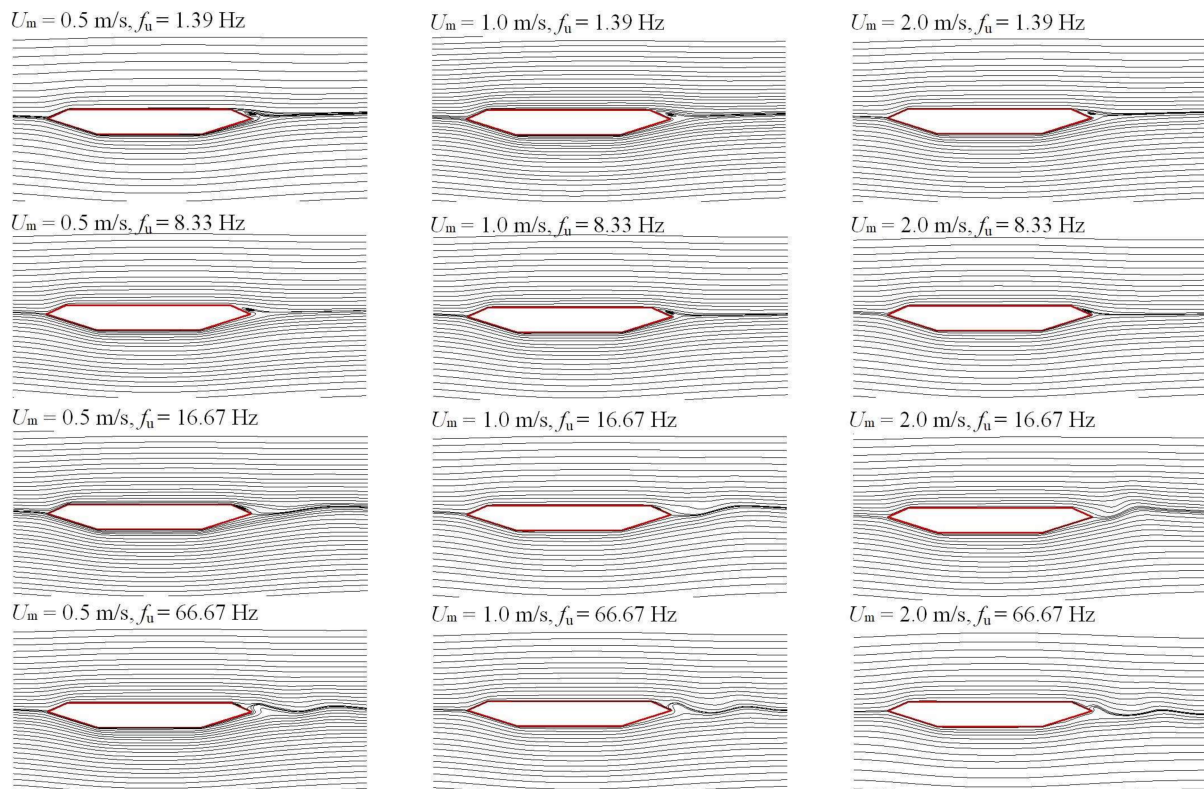


Figure 14. The effect of U_m and f_u on time-averaged stream line distributions in streamwise oscillating flows.

5.2. Wake Characteristics

Figure 15 shows the instantaneous wake vorticity distributions of the box girder in different streamwise sinusoidal flow fields. Figure 15(a₁–a₅) present the wake characteristics of the box girder in the harmonic flow fields with different f_u values. It can be observed that the wake in the harmonic flow fields with $f_u \leq 8.33$ Hz is similar to that in the uniform flow field, and the wake does not exhibit an alternate shedding vortex. With the increase in f_u , there are slight alternate shedding vortices in the wake at $f_u = 16.67$ Hz. Moreover, when the oscillating frequency of the flow field is $f_u \geq 33.33$ Hz, obvious alternate shedding vortices can be observed in the wake, which is similar to the ‘2S’ pattern, known as ‘Karman Vortex Street’.

On the other hand, Figure 15(b₁–b₅) present the wake characteristics of the box girder in the harmonic flow fields with different U_m values. According to the comparisons between Figure 15(a₄) and Figure 15(b₄), it can be observed that the oscillating amplitude of the flow has significant effects on the wake, and the larger the amplitude the more obvious the wake vortex shedding.

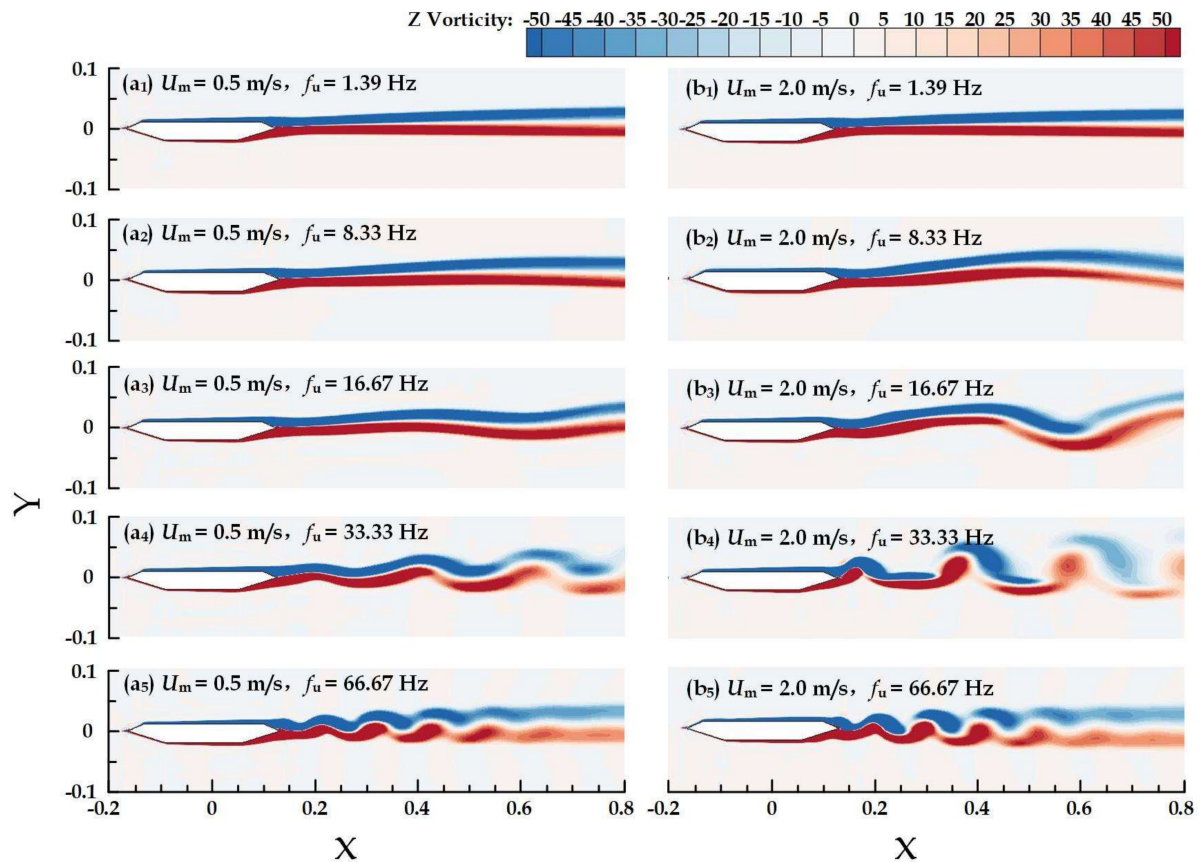


Figure 15. Vortex shedding in sinusoidal oscillating flows: (a₁) $U_m = 0.5$ m/s, $f_u = 1.39$ Hz; (a₂) $U_m = 0.5$ m/s, $f_u = 8.33$ Hz; (a₃) $U_m = 0.5$ m/s, $f_u = 16.67$ Hz; (a₄) $U_m = 0.5$ m/s, $f_u = 33.33$ Hz; (a₅) $U_m = 0.5$ m/s, $f_u = 66.67$ Hz; (b₁) $U_m = 2.0$ m/s, $f_u = 1.39$ Hz; (b₂) $U_m = 2.0$ m/s, $f_u = 8.33$ Hz; (b₃) $U_m = 2.0$ m/s, $f_u = 16.67$ Hz; (b₄) $U_m = 2.0$ m/s, $f_u = 33.33$ Hz; (b₅) $U_m = 2.0$ m/s, $f_u = 66.67$ Hz.

6. Conclusions

In this study, active-control wind tunnel experiments and numerical simulations were conducted to investigate the effects of oscillating frequencies and amplitudes on the pressure distribution and wake characteristics, as well as total force, of a closed box girder. The main conclusions are as follows:

- (1) The time-averaged flow separation and mean pressure coefficients of the closed box girder are insensitive to the oscillating frequency and amplitude of the sinusoidal oscillating inflow. However, the characteristics of the sinusoidal oscillating inflow influence the fluctuating pressure coefficients significantly;
- (2) The inflow oscillating frequency and amplitude have a significant influence on the fluctuating lift and drag forces. The fluctuating drag forces increase linearly with the oscillating frequency;
- (3) The wake vortex shedding is highly correlated to the inflow oscillating frequency and amplitude. There are three significant vortex shedding modes, and more obvious vortex shedding can be observed with higher inflow oscillating frequencies and amplitudes.

Author Contributions: Funding acquisition, L.Z.; Methodology, H.L.; Software, Z.X.; Supervision, L.Z.; Writing—original draft, H.L.; Writing—review & editing, B.W. All authors have read and agreed to the published version of the manuscript.

Funding: This research work was supported by the National Natural Science Foundation under grant numbers 51778093, the Graduate Scientific and Innovation Foundation of Chongqing, China under grant number CYB20028, and the Science and Technology Research Program of the Chongqing Municipal Education Commission under grant number KJZD-K201905201, and the Natural Science Foundation of Chongqing under grant number cstc2021jcyj-bshX0061.

Institutional Review Board Statement: Not applicable.

Informed Consent Statement: Not applicable.

Data Availability Statement: Data are contained within this article.

Conflicts of Interest: The authors declare that there are no conflicts of interest regarding the publication of this paper.

References

1. Xin, J.Z.; Jiang, Y.; Zhou, J.T.; Peng, L.L.; Liu, S.Y.; Tang, Q.Z. Bridge deformation prediction based on SHM data using improved VMD and conditional KDE. *Eng. Struct.* **2022**, *261*, 114285. [[CrossRef](#)]
2. Tang, Q.Z.; Xin, J.Z.; Jiang, Y.; Zhou, J.T.; Li, S.J.; Chen, Z.Y. Novel identification technique of moving loads using the random response power spectral density and deep transfer learning. *Measurement* **2022**, *195*, 111120. [[CrossRef](#)]
3. Li, H.H.; Zhang, L.L.; Wu, B.; Ni, Z.J.; Yang, Y. Effects of the angle of attack on the aerodynamic characteristics of a streamlined box girder. *Adv. Struct. Eng.* **2021**, *24*, 2090–2104. [[CrossRef](#)]
4. Zhu, S.; Li, Y.; Shen, J.; Zhan, Y. Optimization of vortex-induced vibration of flat steel box girders at large attack angle by wind tunnel test. *China Civ. Eng. J.* **2015**, *48*, 79–86. (in Chinese). [[CrossRef](#)]
5. Li, H.H.; Zhang, L.L.; Wu, B.; Yang, Y.; Xiao, Z. Investigation of the 2D Aerodynamic Admittances of a Closed-Box Girder in Sinusoidal Flow Field. *KSCE J. Civ. Eng.* **2021**, *26*, 1267–1281. [[CrossRef](#)]
6. Wu, B.; Li, S.; Li, K.; Zhang, L.L. Experimental determination of the two-dimensional aerodynamic admittances of a 5:1 rectangular cylinder in streamwise sinusoidal flows. *J. Wind Eng. Ind. Aerodyn.* **2021**, *210*, 104525. [[CrossRef](#)]
7. Cao, S.Y.; Ming, L. Numerical study of flow over a circular cylinder in oscillatory flows with zero-mean and non-zero-mean velocities. *J. Wind Eng. Ind. Aerodyn.* **2015**, *144*, 42–52. [[CrossRef](#)]
8. Morison, J.R.; O'Brien, M.P.; Johnson, J.W.; Schaaf, S.A. The force exerted by surface waves on piles. *J. Pet. Technol.* **1950**, *2*, 149–154. [[CrossRef](#)]
9. Keulegan, G.; Carpenter, L. Forces on cylinders and plates in an oscillating fluid. *J. Res. Natl. Inst. Stand. Technol.* **1958**, *60*, 423. [[CrossRef](#)]
10. Williamson, C. Sinusoidal flow relative to circular cylinders. *J. Fluid Mech.* **1985**, *155*, 141–174. [[CrossRef](#)]
11. Obasaju, E.D.; Bearman, P.W.; Graham, J.M.R. A study of forces, circulation and vortex patterns around a circular cylinder in oscillating flow. *J. Fluid Mech.* **1988**, *196*, 467–494. [[CrossRef](#)]
12. Nomura, T.; Suzuki, Y.; Uemura, M.; Kobayashi, N. Aerodynamic forces on a square cylinder in oscillating flow with mean velocity. *J. Wind Eng. Ind. Aerodyn.* **2003**, *91*, 199–208. [[CrossRef](#)]
13. Chen, C.C.; Fang, F.M.; Li, Y.C.; Huang, L.-M.; Chung, C.Y. Fluid forces on a square cylinder in oscillating flows with non-zero-mean velocities. *Int. J. Numer. Methods Fluids* **2008**, *60*, 79–93. [[CrossRef](#)]
14. Zhao, M.; Cheng, L.; An, H.-W. Three-dimensional numerical simulation of flow around a circular cylinder under combined steady and oscillatory flow. *J. Hydrodyn.* **2010**, *22*, 144–149. [[CrossRef](#)]
15. Ribner, H.S. Spectral theory of buffeting and gust response: Unification and extension. *J. Aeron Sci.* **2015**, *23*, 1075–1077. [[CrossRef](#)]
16. Ma, T.T.; Zhao, L.; Cao, S.Y.; Ge, Y.J.; Miyagi, H. Investigations of aerodynamic effects on streamlined box girder using two-dimensional actively-controlled oncoming flow. *J. Wind Eng. Ind. Aerodyn.* **2013**, *122*, 118–129. [[CrossRef](#)]
17. Wang, J.; Ma, C.; Dragomirescu, E.; Chen, X.; Yang, Y. Two-Dimensional Aerodynamic Admittance of a Flat Closed-Box Bridge. *J. Struct. Eng.* **2021**, *147*, 04020359. [[CrossRef](#)]